

Soft X-ray spectral variability of AM Herculis[★]

K. Beuermann¹, E. El Kholi^{2,1}, and K. Reinsch¹

¹ Institut für Astrophysik, Friedrich-Hund-Platz 1, D-37077 Göttingen, Germany, beuermann or reinsch@astro.physik.uni-goettingen.de,

² National Research Institute of Astronomy and Geophysics, Helwan, Cairo, Egypt, essam@nriag.sci.eg

Received December 28, 2007 / February 12, 2008

ABSTRACT

Context. Polars (AM Herculis binaries) are a prominent class of bright soft X-ray sources, many of which were discovered with *ROSAT*.

Aims. We present a homogenous analysis of all the pointed *ROSAT* PSPC observations of polars subdivided into two papers that discuss the prototype polar AM Her in detail and summarize the class properties of all other polars.

Methods. We derive the high-state soft X-ray flux and short-term spectral variability of AM Her using a new detector response matrix and a confirmed flux calibration of the *ROSAT* PSPC below 0.28 keV.

Results. The best-fit mean single-blackbody temperature and integrated bright-phase energy flux of AM Her in its April 1991 high state are 27.2 ± 1.0 eV and $(2.6 \pm 0.6) \times 10^{-9}$ erg cm⁻²s⁻¹, respectively. The total blackbody flux of a multi-temperature model that fits both the soft X-ray and the fluctuating far-ultraviolet components is $F_{bb} = (4.5 \pm 1.5) \times 10^{-9}$ erg cm⁻²s⁻¹. The total accretion luminosity at a distance of 80 pc, $L_{bb} = (2.1 \pm 0.7) \times 10^{33}$ erg s⁻¹, implies an accretion rate of $\dot{M} = (2.4 \pm 0.8) \times 10^{-10}$ M_⊙ yr⁻¹ for an 0.78 M_⊙ white dwarf. The soft X-ray flux displays significant variability on time scales down to 200 ms. Correlated spectral and count-rate variations are seen in flares on time scales down to 1 s, demonstrating the heating and cooling associated with individual accretion events.

Conclusions. Our spectral and temporal analysis provides direct evidence for the blobby accretion model and suggests a connection between the soft X-ray and the fluctuating far-ultraviolet components.

Key words. Accretion – Stars: cataclysmic variables – Stars: individual: (AM Her) – X-rays: binaries

1. Introduction

Research on polars, the synchronized magnetic variety of cataclysmic variables (CVs), has greatly benefited from the discovery of numerous new members of the class during the *ROSAT* All Sky Survey and the subsequent pointed observations with the position sensitive proportional counter (PSPC) (Beuermann & Thomas 1993). As a prominent example, we discuss the statistically highly significant PSPC spectrum of the prototype polar AM Her and its short-term spectral variability. The second paper of this short series of two summarizes the spectral analysis of all other polars observed with the *ROSAT* PSPC. Before embarking on this project, we have investigated the putative absolute miscalibration of the PSPC by up to a factor of two at photon energies below the interstellar carbon edge at 0.28 keV (Napiwotzki et al. 1993; Jordan et al. 1994; Wolff et al. 1996, 1999), where most of the energy flux of polars resides. We use the new in-flight calibration of the PSPC for such low-energy photons (Beuermann et al. 2006; Beuermann 2008) and a corrected detector response matrix of the PSPC that removes defects in the spectra of very soft sources and leads to improved spectral-fit parameters (Beuermann 2008).

2. ROSAT observations of AM Herculis

AM Her was observed with the PSPC on 12/13 April 1991 for 11.6 ks in its high state and on 15/16 September 1991 for 30.6 ks in an intermediate or low state. Other short exposures exist, but

are not considered here. After the decommissioning of the PSPC, AM Her was repeatedly observed with the high-resolution imager (HRI), on 13–17 March 1994 and 8–10 March 1995 during high states and between 26 January and 30 May 1996, when it declined from a high state into a deep low with zero detectable flux. In all *ROSAT* observations, AM Her was encountered in its normal mode of accretion with the pole that points more directly towards the secondary receiving most or all of the transferred matter. The system is bright for magnetic phases $\phi \simeq 0.2 - 1.0$, where $\phi \simeq 0$ refers to the linear polarization pulse that occurs when the accretion spot crosses the limb of the white dwarf and the line of sight is perpendicular to the magnetic field direction (Heise & Verbunt 1988). Table 1 lists all observations used in this paper along with the AAVSO visual brightness estimates.

3. Results

The April 1991 high-state PSPC observation of AM Her was previously discussed by Ramsay et al. (1996). We concentrate here on three aspects not considered so far, the combined discussion of the soft X-ray and far-ultraviolet spectra, a comparison of the PSPC data with the higher resolved *Chandra* and *EUVE* spectroscopic observations, and the spectral variability on time scales down to 1 s in an attempt to shed light on the heating and cooling processes in the accretion spot.

[★] Based on observations made with the *ROSAT* satellite.

Table 1. Mean AAVSO magnitudes for the AM Her observations used in this paper. The date is for the start of exposure. H and L refer to high and low states, respectively.

Instrument	Date	Exp (ks)	State	Magnitude [†]	Ref.
ROSAT PSPC	1991-04-12	11.6	H	13.0 ± 0.2	(1)
PSPC	1991-09-15	30.6	L	15.0	
HRI	1996-01-26	2.3	H	13.2	
EUVE	1993-09-23	74.0	H-	13.5 ± 0.2	
	1995-03-08	121.0	H	13.1 ± 0.2	
HUT	1995-03-09	6.7	H	13.1 ± 0.2	(2)
Chandra LETG	2000-03-09	24.0	H	13.3 ± 0.2	(3)

[†] The 'magnitude' is the average of the AAVSO readings over the duration of the observation and the 'error' is their standard deviation. References: (1) Gänsicke et al. (1995), (2) Greeley et al. (1999), (3) Burwitz et al. (2002), Trill (2006).

3.1. Mean bright phase PSPC spectrum of AM Her

We fit the high-state bright-phase spectrum of AM Her by the sum of three terms: (i) a thermal bremsstrahlung component with a fixed temperature of 20 keV, (ii) a Raymond-Smith thermal spectrum with a fitted temperature of 0.18 keV that accounts for the line emission known to exist at $E < 1$ keV, and (iii) a quasi-blackbody component that fits the soft X-ray emission. The actual value of the bremsstrahlung temperature is not relevant for the fit to the PSPC spectrum. The integrated bremsstrahlung flux, however, is relevant and the value quoted below is taken from the fits to the Ginga, ASCA, and RXTE spectra (Beardmore et al. 1995; Ishida et al. 1997; Christian 2000). For simplicity, we describe interstellar absorption by a column density of cold gas with solar composition, neglecting both the finite ionization of the gas and the condensation of metals into dust. In this spirit, we do not include the ionization edge at 85 Å present in the *EUVE* and *Chandra* LETG spectra (Paerels et al. 1996; Trill 2006). Different assumptions will slightly change the derived blackbody temperature, but leave the general conclusions unaffected. Our value of the column density for AM Her falls within the range of earlier results (Paerels et al. 1996; Ramsay et al. 1996; Trill 2006) and, as those, exceeds the interstellar Ly α -derived atomic hydrogen column density $N_{\text{Ly}\alpha} = (3.0 \pm 1.5) \times 10^{19}$ H-atoms cm⁻² (Gänsicke et al. 1995), suggesting additional intra-binary absorption.

A fit to the mean bright-phase ($\phi = 0.22 - 0.86$) *ROSAT* PSPC spectrum using the above model and the nominal detector response matrix DRMPSPC-AO1 yields excessive residuals in channels 10 to 40 ($E = 0.10 - 0.40$ keV) with peak and rms values of 7.6σ and 3.6σ , respectively (Fig. 1, bottom panel). These residuals largely disappear with the revised matrix DRMPSPC-AO1c derived by Beuermann (2008) and adopted here (Fig. 1, center panel) and the reduced χ^2 drops from an unacceptable $\chi^2_{\nu} = 6.57$ to 0.63 (channels 9 to 40), substantially increasing the confidence in the fit. The best-fit single-blackbody temperature, cold-matter column density, and total blackbody flux are $kT_{\text{bb},1} = 27.3 \pm 1.0$ eV, $N_{\text{H}} = (6.3 \pm 0.8) \times 10^{19}$ H-atoms cm⁻², and $F_{\text{bb},1} = (2.6 \pm 0.2) \times 10^{-9}$ erg cm⁻²s⁻¹, respectively, where the errors refer to the 99% confidence limit. Since individual sections of the soft X-ray emitting spot heat and cool independently, the one-temperature fit must be considered a first approximation and the total flux may differ if a range of temperatures is assumed. We consider adding components with a higher and lower temperature in turn. The addition of a blackbody fixed at

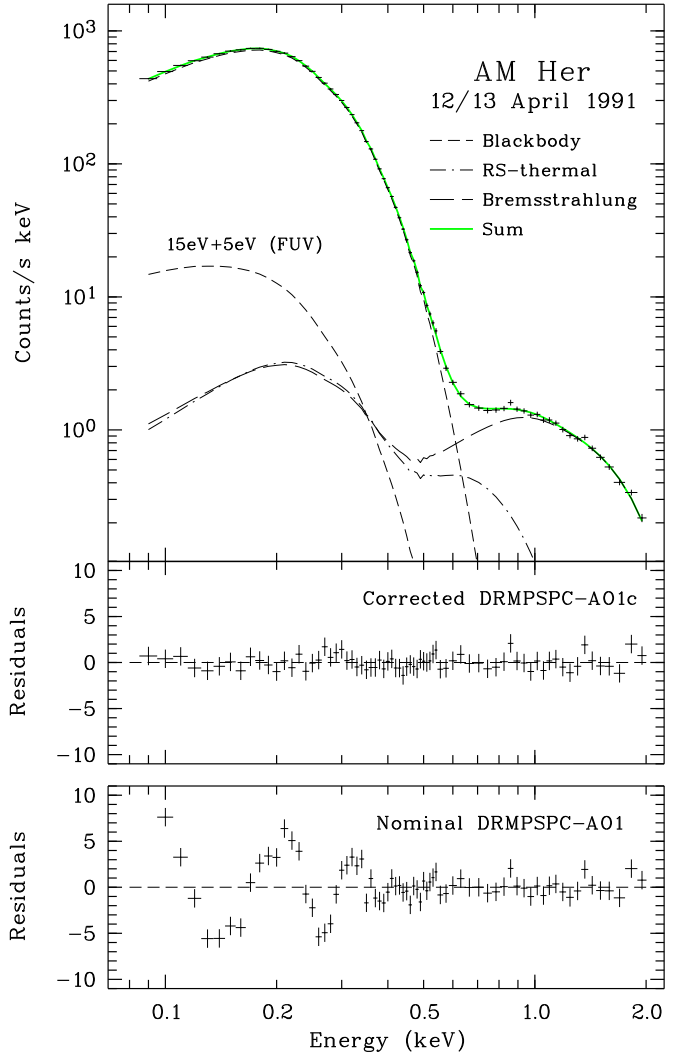


Fig. 1. Bright-phase PSPC spectrum of AM Her in the April 1991 high state. *Top:* Spectral fit of a four-component spectrum to the data using the corrected detector response matrix DRMPSPC-AO1c. The dominant blackbody component has $kT_{\text{bb}} = 27.2$ eV, the minor components have 15 eV and 5 eV. The bremsstrahlung component has $kT_{\text{brems}} = 20$ keV and the low-energy thermal spectrum 0.18 keV. *Center and bottom:* Residuals of the fits obtained with the corrected and the nominal matrix, respectively.

$kT_{\text{bb},2} = 35$ eV (see Sect. 3.3) lowers $kT_{\text{bb},1}$ and raises $F_{\text{bb},1}$, but raises χ^2 , too. At the 95% confidence level, $kT_{\text{bb},1} > 22$ eV and $F_{\text{bb},1} < 5 \times 10^{-9}$ erg cm⁻²s⁻¹. Adding components with lower temperatures requires a discussion of the limit that can be placed on the soft X-ray contribution to the observed ultraviolet flux.

3.2. The ultraviolet limit

The question whether the observed ultraviolet flux represents the Rayleigh-Jeans tail of the soft X-ray quasi-blackbody emission has been debated since the discovery of AM Her as a soft X-ray source (Tuohy et al. 1978, 1981). Important steps towards an answer are the discussion of the energy balance by Gänsicke et al. (1995, 1998) and the detection of rapid fluctuations in the far-ultraviolet flux by Greeley et al. (1999), which lead to the following picture. The white dwarf in AM Her possesses a large UV-bright spot that covers about 10% of the white

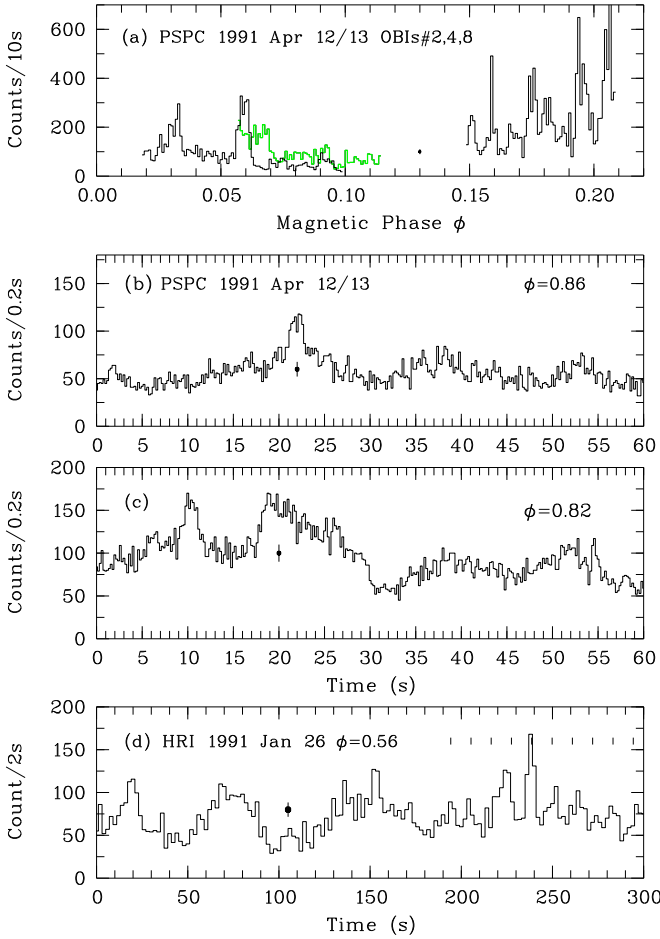


Fig. 2. Short-term X-ray variability of AM Her. (a) PSPC light curve through the orbital dip in the April 1991 high state. Time bins are 10 s. For clarity, one observation interval is shown in green. (b) and (c) One-minute sections near peak flux. Time bins are 200 ms. (d) Section of the HRI light curve in the 1996 high state. Time bins are 2 s. For all panels, the typical statistical uncertainty is indicated by the filled circle with error bars.

dwarf surface (full opening angle 70° , radius 5×10^8 cm). In the high state, it is heated to a central temperature of about 50000 K by bremsstrahlung and cyclotron emission from the hot post-shock plasma located some 10^8 cm above the surface (Gänsicke et al. 1995). The rise from 50000 K to the fluctuating 300000-K spotlets of the soft X-ray emission occurs within a much more restricted region and is largely due to irradiation by soft X-rays. The energy release in soft X-rays exceeds that in bremsstrahlung by an order of magnitude, but the emission occurs at low height. The impact of a dense blob of matter compresses the photospheric plasma in the respective flux tube and radiative heating elevates the photosphere in the immediate surroundings creating a mound (Litchfield & King 1990) of up to several 10^6 cm height. Decompression of a previously mass-loaded flux tube produces a splash that may reach 10^7 cm. The hot matter elevated by these effects may irradiate a spot of about 10^8 cm radius. We identify this emission with the rapidly fluctuating ‘flare-minus-nonflare’ far-ultraviolet component of Greeley et al. (1999), which has a mean high-state bright-phase spectral flux at 930\AA of $1.6 \times 10^{-13} \text{ erg cm}^{-2} \text{ s}^{-1} \text{ \AA}^{-1}$ (Greeley et al. 1999, see his Figs. 7, 9, and 10). Corrected for extinction, this number rises to $1.85 \times 10^{-13} \text{ erg cm}^{-2} \text{ s}^{-1} \text{ \AA}^{-1}$. The

‘flare-minus-nonflare’ component extends to beyond 1800\AA and contains temperatures as low as about 5 eV.

We quote two combinations of three blackbodies each that both match the PSPC spectrum *as well as* the far-ultraviolet spectral slope and flux at 930\AA and embrace the plausible range of parameters: (i) a combination of 27.2 eV, 15 eV and 5 eV (Fig. 1, top panel) has a total blackbody flux of $F_{\text{bb}} = 3.6 \times 10^{-9} \text{ erg cm}^{-2} \text{ s}^{-1}$ and (ii) the less well fitting combination of 35 eV, 22 eV, and 5 eV has $F_{\text{bb}} = 5.5 \times 10^{-9} \text{ erg cm}^{-2} \text{ s}^{-1}$. The dominant contributors to the PSPC spectrum and to F_{bb} are the components with 27 eV and 22 eV, respectively. We conclude that, although there is some freedom, the total high-state blackbody flux is confined to $F_{\text{bb}} = (4.5 \pm 1.5) \times 10^{-9} \text{ erg cm}^{-2} \text{ s}^{-1}$, with an error that encompasses also the variations between individual high states (Hessman et al. 2000).

3.3. The EUVE and Chandra LETG spectra

The mean EUVE and the Chandra LETG spectra¹ agree within their uncertainties and the PSPC spectrum, although poorly resolved, is entirely consistent with the Chandra LETG spectrum as demonstrated by Beuermann (2008). Single-blackbody fits to the individual spectra have yielded $kT_{\text{bb}} = 19.0 - 22.8 \text{ eV}$ for EUVE (Paerels et al. 1996; Christian 2000) and $kT_{\text{bb}} = 31.7 \text{ eV}$ for Chandra (Trill 2006), with the PSPC temperature falling in between. The low EUVE temperature may result from the limited wavelength range, over which the fit was performed, and to a flux deficit relative to the LETG spectrum between 70 and 80\AA , where the background is high. The single-blackbody fit to the Chandra LETG spectrum is poor and a second component with a lower temperature is required. Surprisingly, the simple model of two blackbodies plus a high-energy thermal component suffices to obtain an adequate fit over the entire wavelength range from $\sim 20\text{\AA}$ to the interstellar cut-off at $\sim 125\text{\AA}$ if one averages over the emission and absorption features (Trill 2006). Trill’s best-fit parameters are $N_{\text{H}} = 8.8 \times 10^{19} \text{ H-atoms cm}^{-2}$, $kT_1 = 35.9 \text{ eV}$, and $kT_2 = 15.3 \text{ eV}$, of which the latter is uncertain being kept from running to a lower value by an ultraviolet constraint that is less restrictive than ours. If we use our constraint, the total energy flux stays within the range quoted above. The detailed spectral structure of the Chandra LETG spectrum is difficult to interpret. Both, a well exposed spectrum and improved model spectra of irradiated atmospheres are needed to proceed.

3.4. Luminosity and accretion rate

With some additional assumptions, the soft X-ray flux allows an estimate of the accretion rate. The concept of soft X-ray emitting matter above the mean photospheric level suggests that emission occurs more or less uniformly into half space (see also Heise et al. 1985) and $L_{\text{bb}} = \eta d^2 F_{\text{bb}}$ with $\eta \simeq 2\pi$, $F_{\text{bb}} = (4.5 \pm 1.5) \times 10^{-9} \text{ ergs}$, and $d \simeq 80 \text{ pc}$ (Thorstensen 2003; Beuermann 2006). In addition, the accretion-induced luminosity L_{acc} includes the cyclotron emission with $F_{\text{cyc}} \simeq 1.1 \times 10^{-10} \text{ erg cm}^{-2} \text{ s}^{-1}$ and $\eta \simeq 2\pi$, and the emission from the accretion stream with $F_{\text{str}} \simeq 1.7 \times 10^{-10} \text{ erg cm}^{-2} \text{ s}^{-1}$ and η probably also near 4π . The bolometric hard X-ray flux in the high state of AM Her is estimated at $2.4 \times 10^{-10} \text{ erg cm}^{-2} \text{ s}^{-1}$ by Ishida et al.

¹ Average of the EUVE nighttime spectra 9309231757N, 9309260306N, and 9503081219N, and the Chandra LETG+HRCS observation 6561 (see Table 1).

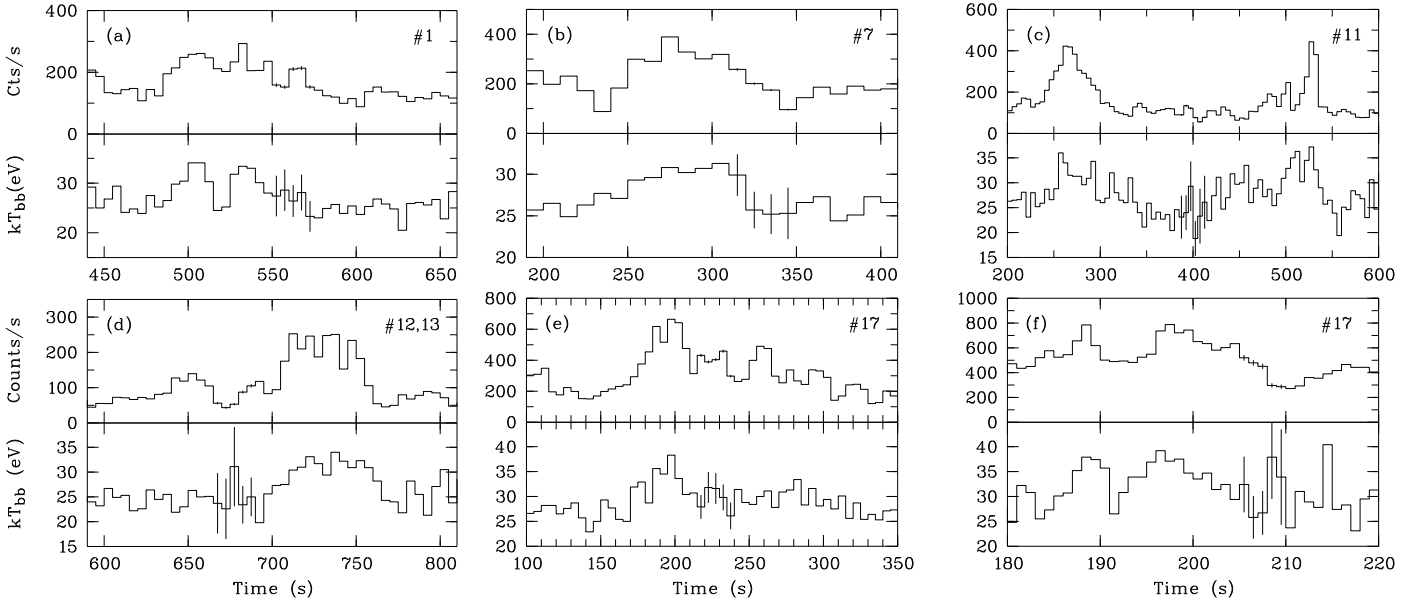


Fig. 3. Short-term spectral variability of AM Herculis through individual flares in the April 1991 high state observation. Plotted is the PSPC count rate and the fitted blackbody temperature vs. time with a time resolution of 10 s in panel *b*, 5 s in panels *a*, *c*, *d*, and *e*, and 1 s in panel *f*. Times start at the beginning of the observation interval (OBI) indicated in the figures.

(1997) from ASCA data, at more than $2.3 \times 10^{-10} \text{ erg cm}^{-2} \text{ s}^{-1}$ by Beardmore et al. (1995) from the Ginga spectrum (the number refers to 2–30 keV in a moderately high state with $V = 13.7$), and at $6.4 \times 10^{-10} \text{ erg cm}^{-2} \text{ s}^{-1}$ by Christian (2000) using RXTE data extending to 100 keV. The hard X-ray geometry factor is $\eta \approx 3.3\pi$, which accounts for the reflection albedo (van Teeseling et al. 1996). The accretion luminosity then is $L_{\text{acc}} = G\dot{M}\dot{M}/R \approx (2.2 \pm 0.8) \times 10^{33} \text{ erg s}^{-1}$, with $M \approx 0.78 M_{\odot}$ and $T_{\text{eff}} = 19800 \text{ K}$ (Gänsicke et al. 2006) the mass and effective temperature of the white dwarf, and $R \approx 7.5 \times 10^8 \text{ cm}$ its radius for a Wood (1995) model with a thick hydrogen envelope. The implied accretion rate is $\dot{M} = (1.6 \pm 0.6) \times 10^{16} \text{ g s}^{-1} = (2.6 \pm 0.9) \times 10^{-10} M_{\odot} \text{ yr}^{-1}$. The luminosity ratio is $L_{\text{bb}}/(L_{\text{hx}} + L_{\text{cyc}}) \approx 4 \pm 2$.

3.5. X-ray light curves and temporal variability

On short time scales, the bright phase is characterized by enormous flaring, which Hameury & King (1988) have described as the superposition of an average of 15 accretion-induced flares occurring simultaneously within the accretion spot. The orbital dip between $\phi \approx 0.0$ and 0.2 occurs when much of the spot is selfeclipsed by the body of the rotating white dwarf. The folded orbital light curves of hard X-rays ($E \gtrsim 0.5 \text{ keV}$) in the high and low states are shown by Gänsicke et al. (1995, see their Figs. 4a and 5a) and the soft X-ray light curves of the individual observation intervals (OBIs) in the April 1991 high state by Ramsay et al. (1996).

Figure 2 illustrates the large fluctuations that occur in the soft X-ray flux of the April 1991 high state for apparent photon energies $E < 0.6 \text{ keV}$ (channels 10–60). Contrary to earlier observations (e.g. Tuohy et al. 1981) and contrary to the present HRI data, flaring in the April 1991 PSPC observations does not vanish entirely during the orbital minimum implying that the accretion spot rotates just barely out of view (Fig. 2, panel *a*). While it is possible that a fraction of the residual flux around $\phi = 0.1$ is from the second pole (Tuohy et al. 1981; Heise et al. 1985), there is no evidence for such an origin. Substantial variability is known to exist on all time scales

down to below 1 s. Quasi-periodic X-ray pulsations have been reported previously (e.g. Tuohy et al. 1981; Stella et al. 1986) and quite persistent pulsations have been seen in the optical cyclotron flux (Bonnet-Bidaud et al. 1991), but most of what we see in the *ROSAT* data is aperiodic and only short data trains are reminiscent of quasi-periodicity (e.g. panel *d*). The pulsations of about 1 min length in panel *d* seem to have a substructure that is around 10 s in the last pulse (tick marks) and the brightest flares in the April 1991 PSPC observation (panels *b* and *c*) show significant variability in subsequent 200 ms bins. Thus, the accretion flow contains structure on length scales from $L > 10^{10} \text{ cm}$ corresponding to the $> 20\text{-s}$ fluctuations modeled by Hameury & King (1988) down to significant density variations over scales as short as 10^8 cm (200 ms). We have calculated autocorrelation functions (not shown), which confirm this picture showing rapid initial decays, longer tails, and, in part, cosine-exponential shapes with no preferred periodicity. The hard X-ray flux ($E > 0.6 \text{ keV}$) in the high state shows much less variability than the soft X-rays. We searched for correlated variations, but found no convincing example, confirming the result of Stella et al. (1986).

3.6. Short-term spectral variability

The zoo of temporal structure seen in the X-ray light curves imply a stream of matter arriving at the white dwarf surface that is highly structured in space and time. It is generally accepted that the high density in most individual packets of matter allows them to penetrate below the photosphere and heat it from below to a temperature that averages about 25 eV (Kuijpers & Pringle 1982; Frank et al. 1988). To cite a popular picture, the spot looks like a puddle in a heavy rain. The stochastic heating and cooling of the individual segments of the spot has never been observed directly, but the superior statistical accuracy of the PSPC data combined with its (though moderate) energy resolution allows the picture to be verified, at least in part.

Ramsay et al. (1996) have shown that the blackbody temperature in the April 1991 PSPC data rises as a function of count

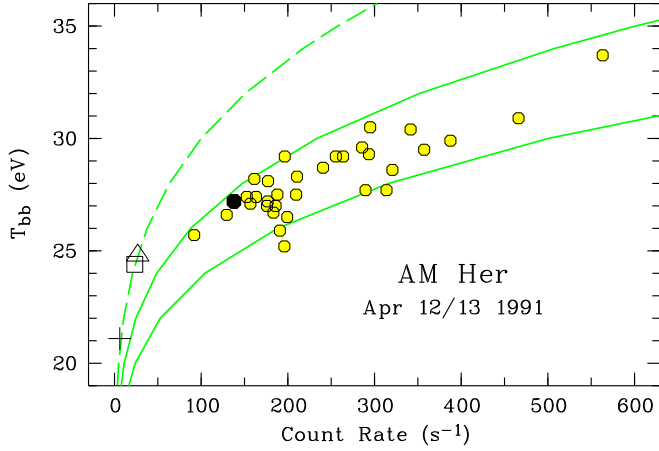


Fig. 4. Best-fit blackbody temperature T_{bb} against the PSPC count rate with time bins of 20 s for the 13 April 1991 high state (OBI 17, open circles). Also shown are the parameters for the mean of the entire bright phase (●), the flares during the egress from the dip (□), the flares in the orbital dip (△), and the orbital dip without flares (+). The curves represent the PSPC count rate vs. T_{bb} dependencies for different projected blackbody emitting areas on the white dwarf.

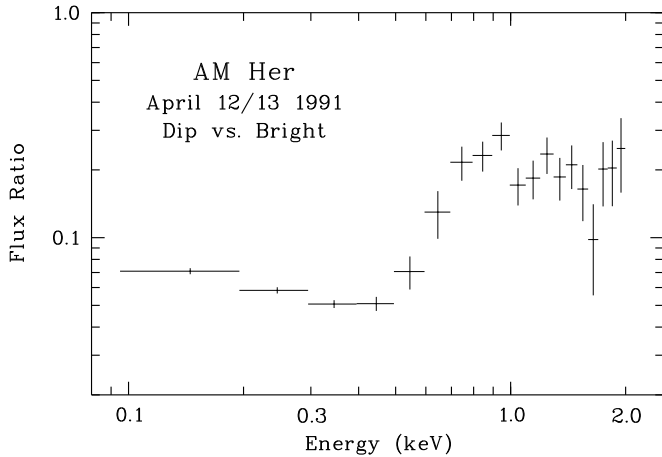


Fig. 5. Ratio of the count rate spectra for the bright phase and the orbital dip of the April 1991 high state observation.

rate or that heating increases with the accretion rate \dot{M} . Ideally, one would like to search for spectral variability as a function of time with time bins that resolve the rapid variations of \dot{M} . With the PSPC, we have established spectral variability in 5 s bins and in the largest flare, we can go down to 1 s. For all spectral fits discussed in this Section, we have adopted a single blackbody plus the hard bremsstrahlung component, both absorbed by a column density fixed at the best-fit value for the mean bright-phase spectrum. This reduction in freedom is necessary, because of the reduced statistics of the short exposures and the strong correlation between the fit parameters kT_{bb} and N_{Hl} . In Fig. 3, we show the fitted blackbody temperature and the PSPC count rate through several flares. Panel *b* has 10 s bins, panels *a*, *c*, *d*, and *e* have 5 s bins, and panel *f* shows the brightest section of the flare in panel *e* at a resolution of 1 s. The correlated increases of temperature and count rate are direct proof that localized sections of the accretion spot are heated by the infall of packets of matter. A one-to-one correspondence is neither observed nor is it expected, because the observed temperature averages over surface

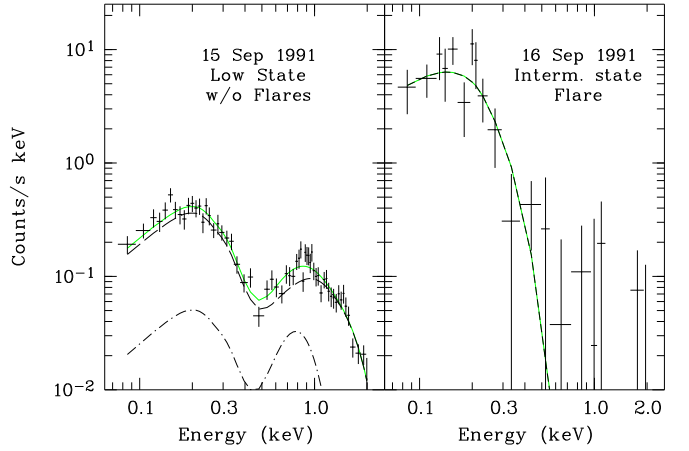


Fig. 6. PSPC spectra of AM Her in the September 1991 low/intermediate state. *Left:* 15 September 1991, low state, bright phase outside flare. *Right:* 16 September 1991, flare minus non-flare count rate spectrum for single soft X-ray dominated event. The signature of the curves is as in Fig. 1.

elements that heat up and cool independently, and the temperature increments differ if a given mass flux is concentrated in a single surface element or distributed over the spot. Fig. 4 depicts the results on the correlation of blackbody temperature vs. count rate for time intervals of 20 s near peak count rate (OBI 17, open circles). Also included are the parameters of the mean bright-phase spectrum (solid circle), the rise from the orbital dip (open square), the flares in the dip (open triangle), and the dip spectrum outside flares (+). The green curves denote the temperature vs. count rate relation for blackbody emission from a projected area A on the surface of the white dwarf absorbed by a column density $N_H = 6.3 \times 10^{19}$ H-atoms cm^{-2} . They refer to a distance of 80 pc and emitting areas $A = 3.4 \times 10^{14}$ cm^2 (dashed curve), 7.9×10^{14} cm^2 (upper solid curve), and 1.69×10^{15} cm^2 (lower solid curve). The mean spectrum (solid circle) corresponds to an emitting area of 8.7×10^{14} cm^2 , which expands in the flares of OBI 17 up to 2×10^{15} cm^2 . During the orbital dip, about 85% of the soft X-ray emitting area disappear behind the limb of the white dwarf.

3.7. Nature of the orbital dip

The fact that flaring ceases more or less completely in the dip suggests that we see some kind of sheet lightning caused by hidden sources behind the limb. This picture is confirmed by the wavelength-dependent ratio of the PSPC spectra for the dip and the bright phase (Fig. 5). The bremsstrahlung flux that dominates the PSPC spectrum at $E > 0.6$ keV is reduced by a factor of only five, whereas the blackbody flux drops by as much as a factor of 20. This spectral behavior follows naturally from the three-dimensional geometry of the emitting region with the heated photosphere disappearing more completely behind the limb than the vertically extended post-shock region. The dip spectrum at $E < 0.5$ keV is decidedly softer than that of the bright phase (Fig. 5, + and ● in Fig. 4), a result that confirms earlier reports by Paerels et al. (1996) and Ramsay et al. (1996). The softer low-energy spectrum in the dip reflects the lower temperature in the outer parts of the spot.

3.8. The September 1991 intermediate and low state

Following the mid-April 1991 flux maximum, AM Her declined into a low state. It was observed with *ROSAT* on 15/16 September 1991 (JD 2448515/6) before it reached minimum visual flux (see Fig. 1 of Hessman et al. 2000 for the AAVSO light curve). On 15 September the X-ray flux was very low and only one substantial flare was observed. The bright-phase spectrum with the flare omitted had a count rate of only 0.18 cts/s. It can be fitted with the Ly α -derived column density of 3×10^{19} H-atoms cm $^{-2}$ and a hard thermal spectrum plus an 0.4 keV thermal component that accounts for the line emission below 1 keV (Fig. 6, left panel). There is no trace of a blackbody component, which implies a count rate below 0.05 cts s $^{-1}$, more than a factor of 2000 lower than in the high state. If the emitting area is the same as in the high state, this factor limits the low-state blackbody temperature to $kT_{\text{bb,low}} \lesssim 12$ eV (based on the upper solid green curve in Fig. 4). The flare on the same day and the generally enhanced flux level on 16 September were also characterized by a hard spectrum, but on 16 September (HJD 2448515.6197) a single large soft X-ray dominated event with an excess count rate of 1.8 cts s $^{-1}$ occurred. Fig. 6 (right panel) shows the spectrum of 88 s of flare exposure minus the enhanced non-flare emission underlying and preceding the flare. This difference spectrum can be fitted by a pure blackbody with a temperature of 21 eV (18 eV) for a cold absorber with $N_{\text{H}} = 3 \times 10^{19}$ (6×10^{19}) H-atoms cm $^{-2}$. The energy released in the flare is $\Delta E \approx 1.1 \times 10^{33}$ erg, created by the infall of about $\Delta M \approx 10^{16}$ g. The energy flux in the high state is larger by a factor of 75 and can be provided by, e.g., 15 flares occurring simultaneously (Hameury & King 1988) that are each larger by a factor of five. Our observations suggest that the lack of soft X-ray emission in the low/intermediate state is due to the rarity of such flares and not to continued flaring at a temperature too low for detection with the PSPC. In summary, the low state is characterized by a tenuous (and occasionally subsiding) flow of accreting matter that goes through a strong shock above the white dwarf surface and cools by optically thin thermal X-ray emission and cyclotron radiation. The intermediate state may be defined by the occurrence of the first dense packets of matter that penetrate the photosphere and the high state by the dominance of blobby accretion. Whether the dense blobs form in the magnetosphere or already in the L $_1$ nozzle is still an unsolved question.

4. Summary

We have analyzed the *ROSAT* PSPC bright-phase spectrum in the high state of AM Her using an improved detector response matrix. The soft part of the PSPC spectrum is consistent with a single blackbody of $kT_{\text{bb}} = 27.4$ eV and a total blackbody flux of $F_{\text{bb}} = 2.6 \times 10^{-9}$ erg cm $^{-2}$ s $^{-1}$. Assuming a range of temperatures and considering the limit set by the variable component of the far-ultraviolet flux (Greeley et al. 1999), we derive the flux of a combination of blackbodies that account for the soft X-ray and the far-ultraviolet flux and includes any blackbody that may hide in the unobservable part of the Lyman continuum: $F_{\text{bb}} = (4.5 \pm 1.5) \times 10^{-9}$ erg cm $^{-2}$ s $^{-1}$. For a distance of 80 pc, the implied accretion luminosity of AM Her is $L_{\text{acc}} = (2.1 \pm 0.7) \times 10^{33}$ erg s $^{-1}$ and the best estimate of the accretion rate is $\dot{M} = (2.4 \pm 0.8) \times 10^{-10} M_{\odot}$ yr $^{-1}$. The spectral parameters reported here are consistent also with the bright-phase high-state spectra of AM Her observed with *EUVE* and the *Chandra* LETG+HRC spectrometers.

We have detected rapid soft X-ray spectral variability through the intense flares in the April 1991 high state of AM Her. In many flares, correlated variations of the blackbody temperature and the PSPC count rate provide proof of the heating and cooling of sections of the accretion spot in response to a locally enhanced accretion rate. The time scale of these variations can be as short as 200 ms, but even at peak count rate we can detect spectral variability only for $\Delta t \geq 1$ s. The Kelvin-Helmholtz time scale of the immediate vicinity of the impact spot is quite short and the time scale of the observed spectral variations is essentially that of the \dot{M} variations. The soft X-ray emitting area of about 10^{15} cm 2 is much smaller than the $\geq 10^{17}$ cm 2 of the ultraviolet spot (e.g. Gänsicke et al. 1995, 1998, 2006). In its low state, AM Her, emits a hard thermal X-ray spectrum supported by a flow of tenuous matter. Occasional infall of denser packets of matter mark the onset of an intermediate state and the dominance of blobby accretion the high state.

Acknowledgements. The anonymous referee has provided constructive comments that improved the presentation of the paper. We thank Vadim Burwitz for giving us the mean *Chandra* LETG spectrum of AM Her and acknowledge with thanks the observations of AM Her from the AAVSO International Database contributed by observers worldwide. EE and KB thank the National Research Institute (NRIAG), Helwan, Egypt, for financial support. EE thanks the Deutscher Akademischer Auslandsdienst (DAAD) for a grant to perform his PhD work within the Channel-Program at the University of Göttingen/Germany. This research was in part funded by the DLR under project number 50 OR 0501.

References

- Beardmore, A. P., Done, C., Osborne, J. P., & Ishida, M. 1995, MNRAS, 272, 749
- Beuermann, K. 2006, A&A, 460, 783
- Beuermann, K. 2008, A&A, in print
- Beuermann, K., Burwitz, V., & Rauch, T. 2006, A&A, 458, 541
- Beuermann, K., & Thomas, H.-C. 1993, Advances in Space Research, 13, 115
- Bonnet-Bidaud, J. M., Somova, T. A., & Somov, N. N. 1991, A&A, 251, L27
- Burwitz, V., Reinsch, K., Haberl, F., Gänsicke, B. T., & Predehl, P. 2002, The Physics of Cataclysmic Variables and Related Objects, ASP Conf. Ser., 261, 137
- Christian, D. J. 2000, AJ, 119, 1930
- Frank, J., King, A. R., & Lasota, J.-P. 1988, A&A, 193, 113
- Gänsicke, B. T., Beuermann, K., & de Martino, D. 1995, A&A, 303, 127
- Gänsicke, B. T., Hoard, D. W., Beuermann, K., Sion, E. M., & Szkody, P. 1998, A&A, 338, 933
- Gänsicke, B. T., Long, K. S., Barstow, M. A., & Hubeny, I. 2006, ApJ, 639, 1039
- Greeley, B. W., Blair, W. P., Long, K. S., & Raymond, J. C. 1999, ApJ, 513, 491
- Hameury, J. M., & King, A. R. 1988, MNRAS, 235, 433
- Heise, J., Brinkman, A. C., Gronenschild, et al. 1985, A&A, 148, L14
- Heise, J., & Verbunt, F. 1988, A&A, 189, 112
- Hessman, F. V., Gänsicke, B. T., & Mattei, J. A. 2000, A&A, 361, 952
- Ishida, M., Matsuzaki, K., Fujimoto, R., Mukai, K., & Osborne, J. P. 1997, MNRAS, 287, 651
- Jordan, S., Wolff, B., Koester, D., & Napiwotzki, R. 1994, A&A, 290, 834
- Kuijpers, J., & Pringle, J. E. 1982, A&A, 114, L4
- Litchfield, S. J., & King, A. R. 1990, MNRAS, 247, 200
- Napiwotzki, R., Barstow, M. A., Fleming, T., Holweger, H., Jordan, S., & Werner, K. 1993, A&A, 278, 478
- Paerels, F., Hur, M. Y., Mauche, C. W., & Heise, J. 1996, ApJ, 464, 884
- Ramsay, G., Cropper, M., & Mason, K. O. 1996, MNRAS, 278, 285
- Stella, L., Beuermann, K., & Patterson, J. 1986, ApJ, 306, 225
- Thorstensen, J. R. 2003, AJ, 126, 3017
- Trill, M. 2006, Masters Thesis, Munich University, and Burwitz, V., et al., in preparation
- Tuohy, I. R., Garmire, G. P., Lamb, F. K., & Mason, K. O. 1978, ApJ, 226, L17
- Tuohy, I. R., Mason, K. O., Garmire, G. P., & Lamb, F. K. 1981, ApJ, 245, 183
- van Teeseling, A., Kaastra, J. S., & Heise, J. 1996, A&A, 312, 186
- Wolff, B., Jordan, S., & Koester, D. 1996, A&A, 307, 149
- Wolff, B., Koester, D., & Lallement, R. 1999, A&A, 346, 969
- Wood, M. 1995, LNP 443, 41

List of Objects

‘AM Her’ on page 1

‘AM Her’ on page 1